Fragmentation of Gamow-Teller strength observed in ^{117,120}Sn(^{3}He,t)^{117,120}Sb charge-exchange reactions

J. Jänecke, K. Pham, D. A. Roberts, and D. Stewart
Department of Physics, University of Michigan, Ann Arbor, Michigan 48109

M. N. Harakeh*
Faculteit Natuurkunde en Sterrenkunde, Vrije Universiteit, 1081 HV Amsterdam, The Netherlands

G. P. A. Berg, C. C. Foster, J. E. Lisantti,† R. Sawafta,‡ and E. J. Stephenson
Indiana University Cyclotron Facility, Bloomington, Indiana 47405

A. M. van den Berg and S. Y. van der Werf
Kernfysisch Versneller Instituut, 9747 AA Groningen, The Netherlands

S. E. Muraviev and M. H. Urin
Engineering Physics Institute, 115 409 Moscow, Russia
(Received 1 July 1993)

The (^{3}He,t) charge-exchange reaction has been studied at $E(^3\text{He})$=200 MeV and angles near 0° on targets of ^{117}Sn and ^{120}Sn. Fragmentation of the giant Gamow-Teller resonance into separate components of the particle-hole type has been observed in good agreement with theoretical predictions. These components are connected with what is usually referred to in the literature as direct-, core-polarization-, and back-spin-flip Gamow-Teller strength. The observed cross sections near $\theta = 0°$ suggest contributions from the isovector spin-flip interaction as well as the isovector tensor interaction. A theoretically predicted configuration splitting of the main Gamow-Teller component into two components involving the $1h_{11/2}$ neutron orbital could not uniquely be identified. The data are compatible, though, with such a splitting since the observed widths of the main Gamow-Teller components in ^{117}Sb and ^{120}Sb exceed the predicted splittings.

PACS number(s): 25.55.Kr, 24.30.Cz, 27.60.+j

I. INTRODUCTION

Theoretical discussions of properties of Gamow-Teller (GT) resonances predate their experimental observation by many years. It appears that Ikeda, Fujii, and Fujita [1] were the first to recognize the possibility of the existence of collective 1^+ states with structures related to isobaric analog states (IAS's). Gaponov and Lyutostanskii [2,3] derived in a quasiclassical treatment many properties of the high-lying 1^+ states of maximum collectivity associated mainly with excitations of neutrons from $j = l + \frac{1}{2}$ orbits into protons in $j = l - \frac{1}{2}$ orbits (spin-orbit partners). Whereas an energy difference E_x(GT) $-E_x$(IAS) of 3–6 MeV was suggested for medium-heavy nuclei, the difference was predicted to approach zero for nuclei with large mass numbers A and large neutron excesses $N - Z$. This behavior was indeed observed later with E_x(GT) $\approx E_x$(IAS) for ^{208}Bi. The authors pointed out the importance of the Wigner supermultiplet scheme [4] for a simultaneous description of spin-isospin characteristics. Using a simplified shell-model version of spin-isospin transitions (a so-called "three-level model"), they further predicted the existence of low-lying Gamow-Teller fragments associated with $j \rightarrow j$ core-polarization and (in neutron-rich nuclei) $j = l - \frac{1}{2} \rightarrow j = l + \frac{1}{2}$ back-spin-flip transitions. For GT resonances based on the ground states of the Sn isotopes, the strength of the latter components was estimated to range from 10% to 25% of the GT sum rule. A configuration splitting of the main Gamow-Teller component has also been predicted recently by Guba, Nikolaev, and Urin [5] for the Ge and Sn isotopes. It is related to the filling of the $1g_{\frac{9}{2}}$ and $1h_{\frac{11}{2}}$ neutron orbits in the respective nuclei.

The initial observation of experimental Gamow-Teller strength below the isobaric analog states, primarily in light nuclei (e.g., Refs. [6–9]), was followed by the early investigations with the (p,n) charge-exchange reaction at proton energies of 25–45 MeV reported by a group at Michigan State University [10–13]. Systematic studies at higher bombarding energy [14–16] were begun in the early 1980s. The observation of Gamow-Teller resonances was facilitated by the realization that at bombarding energies > 100 MeV and angles of $\approx 0°$, i.e., corresponding to very small momentum transfer, the (p,n)

*Present address: Kernfysisch Versneller Instituut, 9747 AA Groningen, The Netherlands.
†Present address: Centenary College of Louisiana, Shreveport, LA 71134.
‡Present address: Brookhaven National Laboratory, Upton, NY 11973.

charge-exchange reaction preferentially excites collective spin-flip $L = 0$ states, such as the Gamow-Teller resonance. Furthermore, the approximate proportionality between the Gamow-Teller strength $B(\mathrm{GT})$ and 0° cross sections contributed significantly in recent years to the understanding of the GT strength in nuclei [17]. The dependence on mass number of the excitation energies, the widths, and sum-rule values were investigated.

The present work shows that the (^{3}He,t) charge-exchange reaction [18,19] is suited to supplement information extracted from the (p,n) charge-exchange reaction. This is due to certain differences in the characteristics of the reaction mechanisms influenced by the effective ^{3}He-nucleon interaction (spin-flip charge exchange and tensor charge exchange) and by the increased absorption of the ^{3}He projectiles as described by the optical model. Experimental aspects also play a role. The much more favorable detection efficiency and energy resolution of triton ejectiles will, for example, facilitate future decay studies as has already been demonstrated in numerous (^{3}He,tp) experiments [20] on isobaric analog states.

Experimental techniques, the data reduction, and experimental results are presented in Secs. II and III. This is followed in Sec. IV by theoretical considerations and the calculation of the Gamow-Teller strength functions for ^{117}Sn and ^{120}Sn and its fragmentation into particle-hole components. Section V describes the nonresonant and resonant components in the observed spectra, and it presents a discussion of the observed phenomena and a comparison between the experimental and theoretical results.

II. EXPERIMENTAL TECHNIQUES AND DATA REDUCTION

The experiment was carried out at the Indiana University Cyclotron Facility (IUCF) with the K600 high-resolution magnetic spectrometer [21,22,18]. A beam of 200 MeV ^{3}He^{++} particles with a beam current of typically 5 nA (electrical) impinged upon targets of 10 mg/cm^2 thickness. Both the incident beam and the reaction products entered the magnetic spectrometer which was set at an angle $\theta \approx 0°$. Whereas the beam with its lower magnetic rigidity was bent inward where it hit an electrically insulated graphite beam stop, the tritons from the (^{3}He,t) reaction traversed the two dipole magnets and were detected and identified in the focal plane detector [21,22]. Background from beam halo was greatly reduced using carefully adjusted beam optics. Background from reactions in the beam stop was suppressed by adjusting the position of the appropriately designed beam stop.

Particles were identified in the focal plane by measuring their energy-loss signals in two scintillators and by time-of-flight measurements of the particles in the spectrometer (scintillator signal versus rf signal of the cyclotron). Details of the focal-plane detection systems are given in Refs. [21,22,18]. Particularly the ray-tracing capability proved to be very important. While two-dimensional ray tracing has successfully been tested, the simpler ray tracing in only the horizontal direction was sufficient to provide the needed information to construct an angle spectrum. Figure 1 displays such a spectrum obtained with a rectangular aperture and with three shadow bars inserted for the angle calibration. Placing the spectrometer at $\theta = 1°$ and dividing the measured spectra into two contributions with equal solid angles made it possible to simultaneously extract spectra centered near $\theta \approx 0°$ ($0.5° \pm 0.8°$) and $\theta \approx 2°$ ($2.1° \pm 0.8°$). This procedure provides a powerful signature for identifying $L = 0$ strength for both non-spin-flip and spin-flip transitions, because of the strongly forward-peaked angular distributions [see, e.g., the angular distribution for the isobaric analog state observed in ^{120}Sn(^{3}He,t)^{120}Sb, Fig. 12 in Ref. [18]]. Particularly the difference spectra ($\theta = 0°$–$2°$) are very sensitive to $L = 0$ contributions.

The spectra shown below in Figs. 2 and 3 were linearized in energy using appropriate energy calibration points. This becomes necessary when spectra obtained at different magnetic field settings are combined. The construction of overlapping spectra also provides a sensitive test for the algorithm used to obtain angles from the raw data, as it necessitates continuity of the 0° and 2° spectra in the overlap region. The on-line and off-line data reduction was carried out with the program XSYS [23] which allows for effective diagnostics during data taking.

III. EXPERIMENTAL RESULTS

Figures 2 and 3 display triton energy spectra measured for the ^{117}Sn and ^{120}Sn targets. The energy resolution is about 250 keV, mostly due to target thickness. The latter spectrum represents the result for two overlapping spectra obtained at different magnetic-field settings. All spectra are linearized in energy. The spectra (a) and (b)

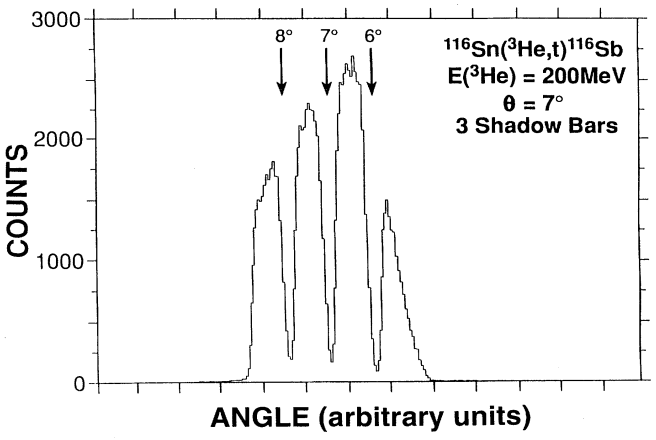

FIG. 1. Test spectrum for extracting angles obtained from a ^{116}Sn(^{3}He,t)^{116}Sb measurement using a rectangular aperture (2.5 cm × 5.0 cm) and three shadow bars (introduced only for angle calibration). The bars are spaced at distances which correspond to $\Delta\theta \approx 1°$. In this calibration measurement the spectrometer was set at 7° with the shadow bars at 6°, 7°, and 8°. The Faraday cup limits the solid angle below $\theta = 6°$.

are centered near $\theta = 0°$ and $\theta = 2°$, respectively. The spectra (c) in both figures represent the differences for the spectra taken at $\theta = 0°$ and that taken at $\theta = 2°$.

The spectra (a) and (b) display a continuous nonresonant background from quasifree charge exchange which is largely canceled in both difference spectra (c), apparently due to a weak dependence on angle. Contributions from another nonresonant continuum background, which is strongly increasing in strength with excitation energy, is also seen in the ^{120}Sn spectra at effective excitation energies above $E_x \approx 30$ MeV. The latter contributions decrease more strongly with angle.

Broad resonances as well as the sharp isobaric analog state at $E_x = 11.3$ MeV in ^{117}Sb and 10.2 MeV in ^{120}Sb (see also Fig. 7 in Ref. [18]) are apparent in all spectra. As expected, the difference spectra (c) enhance the IAS's and certain resonances ($E_x \approx 3$, 6, 12 MeV) with strongly forward-peaked angular distributions which are therefore assigned $L = 0$ angular momentum transfer. One or more resonances at $E_x \approx 19$ MeV appear to have a minimum at $\theta = 0°$.

In addition to the dominating IAS's, other discrete but much weaker states are also observed at low excitation energies. This includes the transition to the ground state of ^{120}Sb. Figure 4 displays a spectrum for the region of low excitation energy for a thin target of ^{120}Sn. Here, the energy resolution is about 130 keV. Several selectively excited sharp states are apparent, and the decomposition into spectra centered near $\theta = 0°$ and 2° (not shown here) identifies some of these as 1^+ states.

All spectra in Figs. 2 and 3 also show calculated curves obtained from a fitting procedure. This will be discussed in Sec. V.

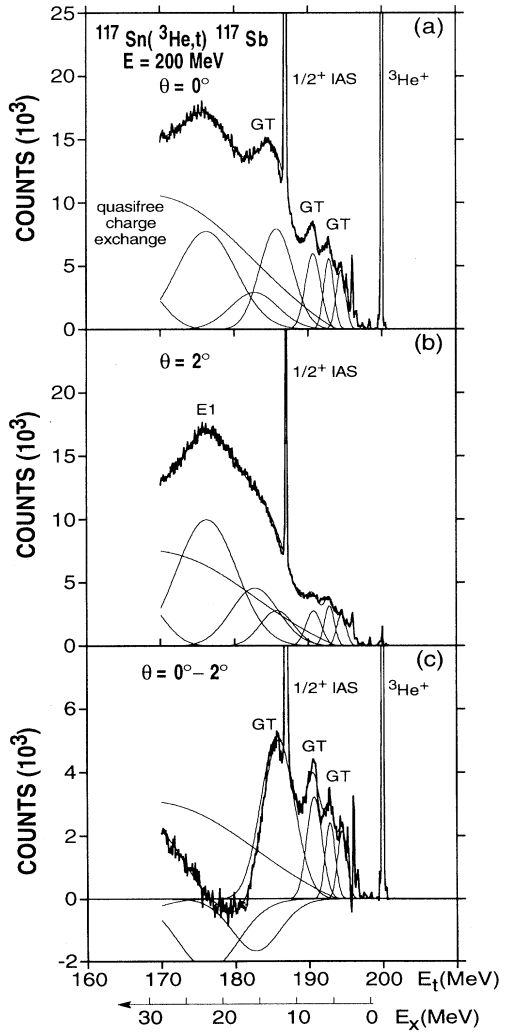

FIG. 2. Triton energy spectra for ^{117}Sn(^{3}He,t)^{117}Sb at $E(^3\text{He}) = 200$ MeV and (a) $\theta \approx 0°$ and (b) $\theta \approx 2°$. Spectrum (c) displays the difference spectrum ($\theta \approx 0°$–2°). The spectra are linearized in energy. The solid curves are obtained from a fitting procedure. They represent nonresonant background and resonances as described in the text.

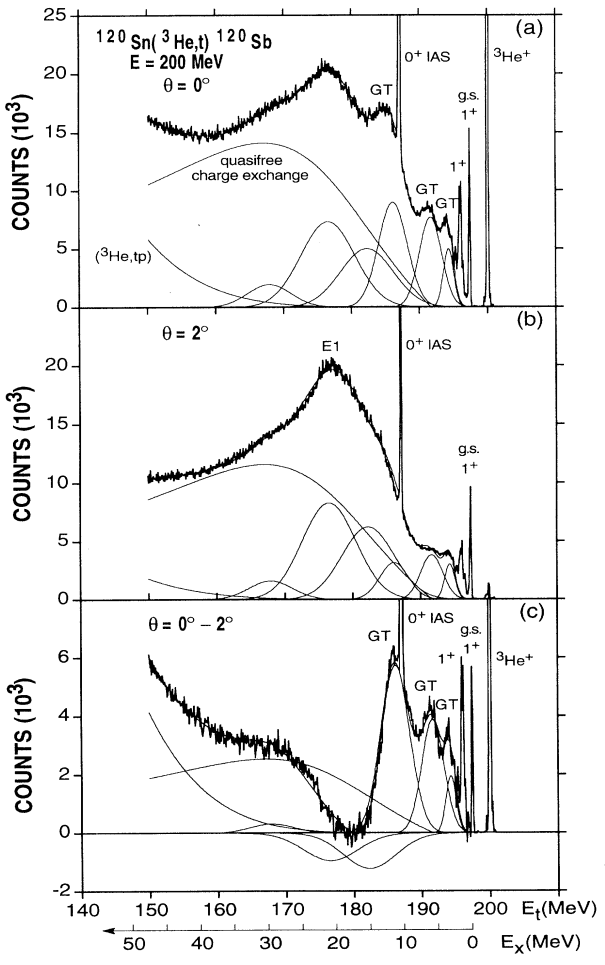

FIG. 3. Triton energy spectra constructed from two overlapping exposures at low and high excitation energies for ^{120}Sn(^{3}He,t)^{120}Sb at $E(^3\text{He}) = 200$ MeV and (a) $\theta \approx 0°$ and (b) $\theta \approx 2°$. Spectrum (c) displays the difference spectrum ($\theta \approx 0°$–2°). The spectra are linearized in energy. The solid curves are obtained from a fitting procedure. They represent nonresonant background and resonances as described in the text.

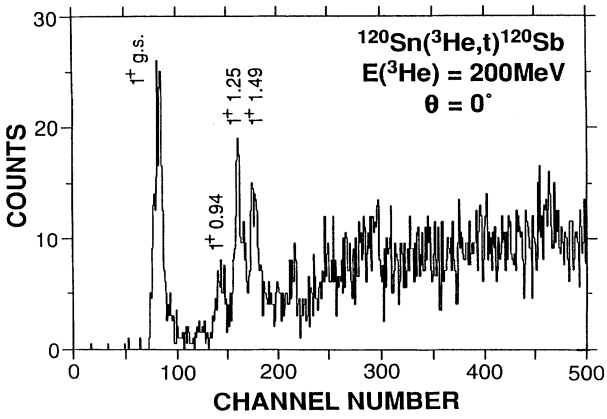

FIG. 4. Triton energy spectrum for ^{120}Sn(^{3}He,t)^{120}Sb at $E(^3\text{He}) = 200$ MeV and $\theta \approx 0°$ for the region of low excitation energy (~ 16.2 keV/channel).

IV. THEORETICAL CONSIDERATIONS

The theoretical description of beta decay and charge-exchange reactions requires the use of Fermi (non-spin-flip) and Gamow-Teller (spin-flip) operators

$$T^{\pm} = \sum_{k=1}^{A} \tau_k^{\pm} \qquad \text{and} \qquad \mathbf{Y}^{\pm} = \sum_{k=1}^{A} \boldsymbol{\sigma}_k \tau_k^{\pm} , \quad (1)$$

where $\boldsymbol{\sigma}$ and $\tau^{\pm}$ are the corresponding Pauli matrices for spin and isospin spaces, respectively. A is the number of nucleons.

The respective reduced transition probabilities for these charge-exchange operators are given by

$$B_{fi}^{\pm}(F) = \frac{1}{2J_i+1} |\langle \Psi_f \| T^{\pm} \| \Psi_i \rangle|^2 , \quad (2)$$

$$B_{fi}^{\pm}(\text{GT}) = \frac{1}{2J_i+1} |\langle \Psi_f \| \mathbf{Y}^{\pm} \| \Psi_i \rangle|^2 , \quad (3)$$

where $|\Psi_i\rangle$ and $|\Psi_f\rangle$ are the wave functions of the initial state of a target nucleus and the final state of a product nucleus, respectively, and J_i is the angular momentum of the initial state.

The above operators, when applied to the ground state of nuclei, result in collective excitations. Isobaric analog states generated by the isospin-lowering operator T^- represent the most coherent superposition of Fermi strength. Similarly, the Gamow-Teller operator $\mathbf{Y}^{\pm}$ induces the excitation of the Gamow-Teller states.

It is interesting to note that important properties of the Gamow-Teller resonances were suggested theoretically prior to the detailed experimental investigations which started in the early 1980s [8–10]. It was pointed out [2,3] that the high-lying 1^+ states of maximum collectivity are mainly associated with charge-exchange excitations of neutrons from orbits with $j = l + \frac{1}{2}$ into protons in the spin-orbit partner orbits with $j = l - \frac{1}{2}$. Considerations involving the Wigner supermultiplet coupling scheme [4] and the spin-isospin characteristics place these excitations at energies near the respective isobaric analog states. If the Wigner SU(4) symmetry is assumed to be exact, the energies of the isobaric analog states and the Gamow-Teller resonances would be equal, and these resonances would exhaust entirely the corresponding sum rules. Under this assumption, the fragmentation of the Gamow-Teller resonance into states of the particle-hole type would not exist. Within the framework of the shell model, the Wigner SU(4) symmetry is broken mainly by the spin-orbit term of the nuclear mean field.

The possible existence of low-lying less collective Gamow-Teller fragments was also predicted on the basis of a quasiclassical treatment within the framework of the random-phase approximation (RPA) [2,3]. Two fragments based on core-polarization spin flip ($j = l \pm \frac{1}{2} \rightarrow j = l \pm \frac{1}{2}$) and back spin flip ($j = l - \frac{1}{2} \rightarrow j = l + \frac{1}{2}$) are expected. The latter type of excitation is present only in neutron-rich nuclei when the proton orbits for a lower-lying spin-orbit partner are not completely filled. Figure 5 shows a schematic representation for the three modes of excitation, and special charge-exchange excitations for Sn isotopes are indicated. For the Sn isotopes the relative strengths for the "pygmy resonances" were estimated by Gaponov and Lyutostanskii [2,3] as (10+0)% (^{114}Sb), (13+1)% (^{116}Sb), (18+2)% (^{118}Sb), (18+4)% (^{120}Sb), (19+5)% (^{122}Sb), and (19+6)% (^{124}Sb), where the two respective numbers refer to the core-polarization and back-spin-flip components, respectively. In a recent reevaluation of the three-level model it was found that these values may be overestimated [24] by a factor of ≈ 2. It is expected from the RPA analysis with the use of a realistic particle-hole basis (as suggested in Fig. 6) that

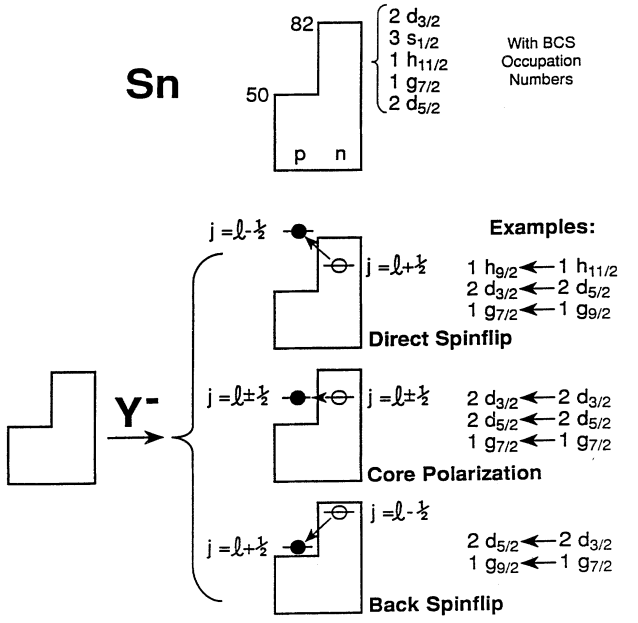

FIG. 5. Schematic representation of particle-hole states excited by the Gamow-Teller operator $Y^{\pm}$. Examples are given for Sn isotopes. Back spin flip occurs in nuclei with large neutron excess.

the number of low-lying Gamow-Teller fragments can be greater than 2.

In addition to the above fragmentation, a configuration splitting of the main Gamow-Teller component was predicted theoretically only recently by Guba *et al.* [5]. A splitting into two collective components of comparable intensities is expected for the resonances based on the ground states of the Ge and Sn isotopes. The splitting should be prominent near the onset of the filling of the $1g_{\frac{9}{2}}$ and $1h_{\frac{11}{2}}$ neutron orbits, respectively.

Gamow-Teller strength functions, defined as the differential excitation probability of a target nucleus due to the external charge-exchange field $\mathbf{Y}^{\pm}$, were calculated for the nuclei ^{117}Sn and ^{120}Sn. According to Eq. (3), the strength function of the Gamow-Teller resonance based on the ground state of the target nucleus $|\Psi_i\rangle$ is defined as

$$S_{\mathrm{GT}}(\omega) = \sum_f B^-_{fi}(\mathrm{GT})\delta(E_f - E_i - \omega). \tag{4}$$

Here, E_f and $E_i(=0)$ are the energies of the final and initial states, respectively. Furthermore, $\omega = E_x + Q$ where ω and E_x are the excitation energies measured from the ground states of the target and final nuclei, respectively.

The continuum RPA is the most advanced method for the description of Gamow-Teller strength within the framework of the particle-hole picture. The RPA equations are briefly given below in the form which is used in the finite Fermi-system theory [25],

$$S_{\mathrm{GT}}(\omega) = -(1/\pi)e_q Im \int A_{\mathrm{GT}}(rr',\omega)V_{\mathrm{GT}}(r',\omega)drdr', \tag{5}$$

$$V_{\mathrm{GT}}(r,\omega) = e_q + (G'/r^2)\int A_{\mathrm{GT}}(rr',\omega)V_{\mathrm{GT}}(r',\omega)dr'. \tag{6}$$

Here, $A_{\mathrm{GT}}(rr',\omega)$ is the radial particle-hole propagator carrying the Gamow-Teller quantum numbers, and $V_{\mathrm{GT}}(r,\omega)\boldsymbol{\sigma}\boldsymbol{\tau}^-$ is the effective field which is different from $e_q\boldsymbol{\sigma}\boldsymbol{\tau}^-$ due to the quasiparticle interaction $\frac{1}{2}G'(\boldsymbol{\sigma}\boldsymbol{\sigma}')(\boldsymbol{\tau}\boldsymbol{\tau}')\delta(\mathbf{r}-\mathbf{r}')$. The quenching effect is taken into account by the local "effective charge" e_q [25]. Since only relative B_{GT} values are considered below, it is possible to set $e_q = 1$. The formula for $A_{\mathrm{GT}}(rr',\omega)$ expressed in terms of single-particle wave and Green functions, energies, and occupation numbers is given, for example, in Ref. [26]. The neutron pairing is taken into account by means of the BCS model.

The energy dependence of the Gamow-Teller strength function (5) exhibits several maxima corresponding to the quasistationary Gamow-Teller states. In the vicinity of the energy of each state $E_{x,f}$, the strength function (5) can be represented in the form

$$S_{\mathrm{GT}}(E_x) = \frac{B_f}{2\pi}\frac{\Gamma^{\uparrow}_f}{(E_x - E_{x,f})^2 + (\Gamma^{\uparrow}_f/2)^2}, \tag{7}$$

where B_f is the Gamow-Teller strength of each state [compare with definition (3)], and $\Gamma^{\uparrow}_f$ is the total escape (proton) width ($\Gamma^{\uparrow}_f = 0$, when $E_{x,f}$ is less than the proton binding energy).

The coupling of the Gamow-Teller states to many-particle many-hole configurations results in a spreading of the considered states. This increases the total width which can be included in Eq. (7) by replacing $\Gamma^{\uparrow}_f$ with $\Gamma_f = \Gamma^{\uparrow}_f + \Gamma^{\downarrow}_f$. Here, Γ_f and $\Gamma^{\downarrow}_f$ are the total and spreading widths of each Gamow-Teller state (the energy shift of the Gamow-Teller states due to the above coupling is neglected). In accordance with the remarks made above, the violation of SU(4) symmetry in nuclei must be taken into account explicitly in the analysis of Gamow-Teller spreading widths. It appears that this problem has not been solved yet. Therefore, to permit a comparison between experimental and theoretical results, a phenomenological spreading width $\Gamma^{\uparrow}_f$ was introduced into Eq. (7). The simplest parametrization of this quantity [27] has the form $\Gamma^{\uparrow}_f = \alpha E^2_{x,f}$, where α is an adjustable parameter. The value of α can be taken from the experimental widths of the Gamow-Teller resonances in other nuclei. Since the spreading of each Gamow-Teller state is expected to be independent of those of others, the Gamow-Teller strength function can be represented as a sum of several Breit-Wigner shapes which correspond to the Gamow-Teller particle-hole states.

The standard set of shell-model parameters has been used in Eqs. (5) and (6) for the calculation of the quantities A_{GT}, V_{GT} and the strength function S_{GT} for the nuclei ^{117}Sn and ^{120}Sn. The parameters of the mean field of the Woods-Saxon type are taken from Ref. [26], and the strength of the pairing interaction is taken from Ref. [28]. These parameters allow one to describe satisfactorily the experimental data of the energies and spectroscopic factors for the low-lying excited states as well as the nucleon binding energies in the Sn isotopes. The strength of the quasiparticle interaction is taken from Ref. [5], $G' = 350$ MeV fm^3, in agreement with the value used in the finite Fermi-system theory [25]. While the Hamiltonian has been diagonalized over the full particle-hole basis, the results for low excitation energies $E_x \leq 3$ MeV are not reliable and are not shown. The calculated strength functions exhibit several resonances which correspond to the Gamow-Teller states.

The energies and strengths of these states are determined from the calculated strength function by means of parametrization (7). These energies and strengths, normalized to 100% for the total strength of the two main components, are included in Tables I and II for comparison with the experimental data for ^{117}Sn and ^{120}Sn, respectively. The Gamow-Teller strength functions which are displayed in the lower part of Figs. 6 and 7 have been calculated by means of Eq. (7) after replacing $\Gamma^{\uparrow}_f \to \Gamma_f = \Gamma^{\uparrow}_f + \Gamma^{\downarrow}_f$ with the use of the data of B_f and $E_{x,f}$ from Tables I and II and the value $\alpha = 0.02$ MeV^{-1}. This value allows one to reproduce the experimental total width of the Gamow-Teller resonance in the ^{140}Ce parent nucleus [29]. It should be noted that the calculated escape widths $\Gamma^{\uparrow}_f$ of all Gamow-Teller states have been found to be less than several keV and can be

TABLE I. Experimental excitation energies, widths, and cross sections from ^{117}Sn(^{3}He,t)^{117}Sb at $E(^3\text{He}) = 200$ MeV. The values given in parentheses assume splitting of the nearby $L = 0$ resonance. Theoretical excitation energies and relative Gamow-Teller transition probabilities are shown in the last two columns. Excitation energies relative to ^{117}Sn are $E_x(^{117}\text{Sn}) = 2.532$ MeV + E_x where the added energy represents the difference in binding energies.

E_x (MeV)	L, J^π	Γ (MeV)	$d\sigma/d\Omega(0°)$ (mb/sr)	$\frac{d\sigma/d\Omega(0°)}{d\sigma/d\Omega(2°)}$	E_x^{calc} (MeV)	GT strength (%)
g.s.	$L = 2, 5/2^+$		0.06±0.01			
2.17±0.11	$L = 0, (3/2^+)$		0.37±0.04	3.2		
3.77±0.05	$L = 0$	1.5±0.1	2.5±0.3	1.9	3.9	3.5
5.41±0.05	$L = 0$	1.6±0.1	3.2±0.3	1.8	4.8	7.7
					6.1	3.6
7.54±0.05	$L = 0$	2.4±0.1	5.3±0.4	2.2	8.0	13
11.27 (IAS)	$L = 0, 1/2^+$		6.7±0.2	3.7		
12.51±0.10	$L = 0$	5.3±0.1	15.2±1.2	2.8		
(11.19±0.10)	$(L = 0)$	(3.7±0.1)	(7.4±0.8)	(3.2)	11.1	60
(13.85±0.10)	$(L = 0)$	(3.8±0.1)	(7.7±0.8)	(2.3)	14.3	40
15.50±0.5	$L = 1$	7.6±0.5	8.0±0.9	0.6		
22.00±0.5	$L = 1$	9.5±0.5	26.7±3.0	0.8		

neglected as compared with the spreading width $\Gamma_f^{\downarrow}$.

Some comments concerning the method and obtained results should be made. (i) The method is similar to that used in Ref. [5]. The difference consists in the procedure of the phenomenological consideration of the Gamow-Teller spreading. A somewhat different G' value has also been used. (ii) As follows from Tables I and II, there are two Gamow-Teller fragments having comparable strength and exhausting the main part of the Gamow-Teller sum rule (the configuration splitting). This result is in agreement with that obtained in Ref. [5]. This splitting is caused by the anomalous difference between the energy of the $1h_{\frac{9}{2}}$-$1h_{\frac{11}{2}}$ proton-neutron hole configuration and the energies of other configurations carrying the Gamow-Teller quantum numbers. This difference is due to the neutron pairing and appears when the neutron $1h_{\frac{11}{2}}$ level is close to the Fermi energy. (iii) As in any quasirandom-phase-approximation (QRPA) calculations of the Gamow-Teller strength function for medium-heavy nuclei, there exist several low-lying Gamow-Teller fragments for ^{117,120}Sn (see Tables I and II). They are slightly collective states of the particle-hole type. The number of these states is determined by the number of the discrete and quasidiscrete Gamow-Teller particle-hole configurations. For ^{117,120}Sn the number of slightly collective states having energies $E_x \geq 3$ MeV are 4 and 3, respectively. In medium-heavy nuclei the Gamow-Teller states closest to the main Gamow-Teller fragment correspond mainly to the direct spin-flip transitions. The Gamow-Teller states corresponding to the core-polarization and back-spin-flip transitions have lower energies. It should be noted that there exist only two weak Gamow-Teller fragments within the framework of the three-level model [2,3,24]. (iv) Because of the dif-

TABLE II. Experimental excitation energies, widths, and cross sections from ^{120}Sn(^{3}He,t)^{120}Sb at $E(^3\text{He}) = 200$ MeV. The values given in parentheses assume splitting of the nearby $L = 0$ resonance. Theoretical excitation energies and relative Gamow-Teller transition probabilities are shown in the last two columns. Excitation energies relative to ^{120}Sn are $E_x(^{120}\text{Sn}) = 3.462$ MeV + E_x where the added energy represents the difference in binding energies.

E_x (MeV)	L, J^π	Γ (MeV)	$d\sigma/d\Omega(0°)$ (mb/sr)	$\frac{d\sigma/d\Omega(0°)}{d\sigma/d\Omega(2°)}$	E_x^{calc} (MeV)	GT strength (%)
g.s.	$L = 0, 1^+$		0.92±0.09	1.5		
0.94±0.03	$L = 0, 1^+$		0.31±0.03	1.8		
1.26±0.03	$L = 0, 1^+$		0.72±0.07	1.8		
1.49±0.03	$L = 0, 1^+$		0.57±0.06	1.8		
3.04±0.05	$L = 0, 1^+$	1.8±0.1	2.8±0.3	1.6	3.5	6.0
					4.3	4.7
5.70±0.05	$L = 0, 1^+$	3.8±0.1	9.3±0.7	2.0	6.3	13
10.20 (IAS)	$L = 0, 0^+$		7.0±0.2	4.1		
11.23±0.10	$L = 0, 1^+$	5.0±0.1	14.1±1.1	2.9		
(10.48±0.10)	$L = 0, 1^+)$	(4.1±0.1)	(9.4±0.8)	(3.1)	9.2	38
(12.90±0.10)	$L = 0, 1^+)$	(3.8±0.1)	(5.3±0.5)	(1.7)	12.6	62
15.1±0.3	$L = 1, (2^-)$	9.1±0.5	14.3±1.6	0.8		
20.8±0.3	$L = 1, 1^-$	9.3±0.5	21.5±2.4	0.9		
≈ 29.4		7.5±0.5	4.6±0.5	1.2		

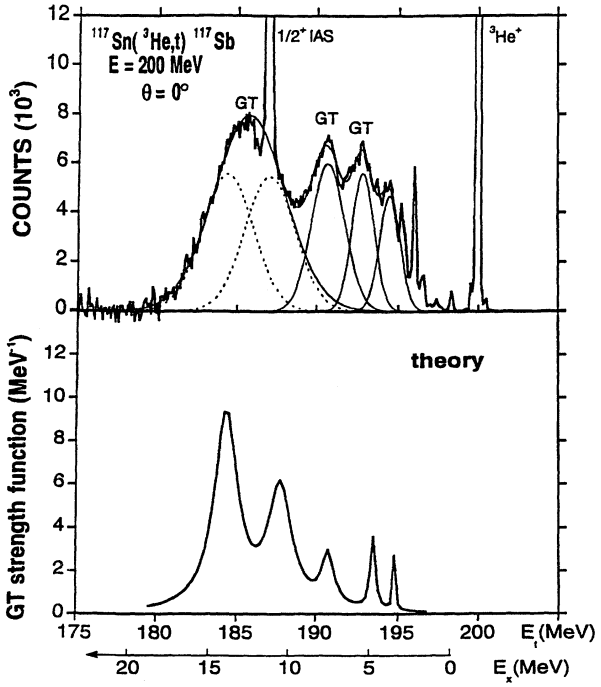

FIG. 6. Top: experimental triton energy spectrum for the giant Gamow-Teller resonances observed in ^{117}Sn(^{3}He,t)^{117}Sb at $E(^3\text{He}) = 200$ MeV and $\theta \approx 0°$. Nonresonant background and giant $\Delta L = 1$ resonances without and with spin flip at higher excitation energies are subtracted for both the experimental data and the fitted spectra. Bottom: Gamow-Teller strength function based on the theoretical calculations from this work. The excitation energies are for the final nucleus ^{117}Sb.

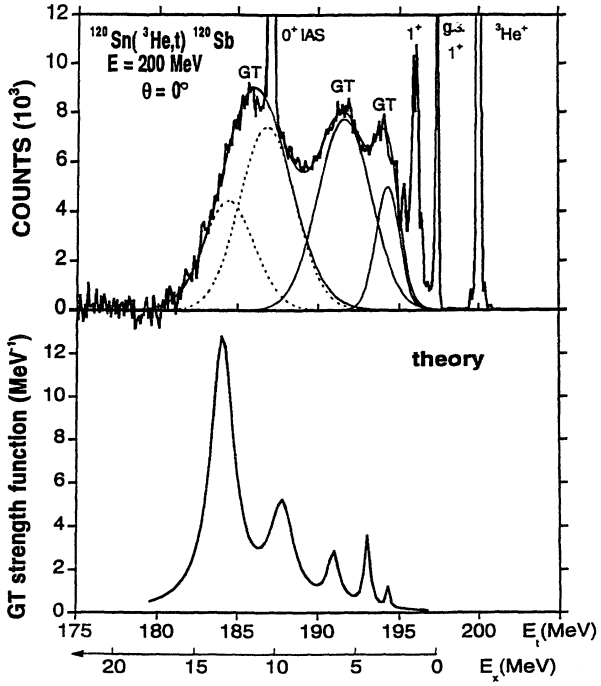

FIG. 7. Top: experimental triton energy spectrum for the giant Gamow-Teller resonances observed in ^{120}Sn(^{3}He,t)^{120}Sb at $E(^3\text{He}) = 200$ MeV and $\theta \approx 0°$. Nonresonant background and giant $\Delta L = 1$ resonances without and with spin flip at higher excitation energies are subtracted for both the experimental data and the fitted spectra. Bottom: Gamow-Teller strength function based on the theoretical calculations from this work. The excitation energies are for the final nucleus ^{120}Sb.

ferent collectivities of the main and weak Gamow-Teller states, one can expect that the transition densities of these states are appreciably different.

It should be noted that other versions of the mean field and quasiparticle interaction as compared to those used by us can be employed in QRPA calculations. This can lead to minor changes in the calculated energies and strengths. The comparison with the experimental results is discussed in Sec. V B.

V. DISCUSSION

A. Nonresonant background

The curves included in Figs. 2 and 3 were obtained by describing the continuous nonresonant background and the resonances with appropriate functions and by optimizing the respective shape parameters.

Quasifree charge exchange is a major source of nonresonant continuum background. Here, the (^{3}He,t) charge-exchange reaction on a bound neutron leads to the ejection of the charge-exchanged proton from the residual nucleus, leaving the residual nucleus in its ground state or in an excited single-neutron hole state. The Fermi motion of the neutron, which interacts with the projectile, will lead to a substantial energy broadening, and the onset of the continuum in the ^{117,120}Sn(^{3}He,tp)^{116,119}Sn reactions is determined by the threshold for three-body breakup. A simple equation used in the study of pion-induced charge exchange [30,31] appears to give a good description of this effect,

$$\frac{d^2\sigma}{dEd\Omega} = N_0 \frac{1-\exp[(E_t - E_0)/T]}{1+[(E_t - E_{\text{QF}})/W]^2}. \quad (8)$$

Here, the centroid energy E_{QF} of the Lorentzian distribution is shifted relative to the energy of the free process, E_t(free), by the proton binding energy S_p, the excitation energy E_{xn} of the neutron-hole state, and the Coulomb barrier B_{Coul} for the proton, $E_{\text{QF}} = E_t(\text{free}) - (S_p + E_{xn} + B_{\text{Coul}})$. The energy E_{xn} is zero only if the neutron is removed from the orbit nearest the Fermi surface. The width W of this distribution is due to the Fermi motion of the neutron inside the target nucleus. The exponential term results from Pauli blocking. The cutoff energy E_0 is fixed by the three-body breakup energy, $E_0 = E_t(\text{g.s.}) - S_p$. The quantity T has the characteristics of a temperature.

The parameters obtained from the global fitting of the nonresonant components in the spectra (a) and (b) of Figs. 2 and 3 are given in Table III. Also given for

TABLE III. Parameters for the semiphenomenological nonresonant continuum background from quasifree charge exchange defined by Eq. (8) for the reactions ^{117,120}Sn(^{3}He,t) at $E(^3\text{He}) = 200$ MeV and comparison with the results from ^{120}Sn(π^+,π^0) at $E(\pi^+) = 165$ MeV and 230 MeV [30,31]. Also given are the cross sections at $\theta \approx 0°$ and 2° and the cross section ratios for the quasifree charge exchange and for the breakup/pickup reaction (see text). The cross sections listed for the former reaction are for the entire energy range, whereas those for the latter represent the integral for energies $E_t \geq 150$ MeV.

	^{117}Sn(^{3}He,t)	^{120}Sn(^{3}He,t)	^{120}Sn(π^+,π^0)	^{120}Sn(π^+,π^0)
Quasifree charge exchange				
$E_{\text{projectile}}$ (MeV)	200	200	165	230
$E_{\text{ejectile(g.s.)}}$ (MeV)	198.236	197.300	167.4	232.4
$E_{\text{ejectile(free)}}$ (MeV)	200.761	200.761	170.4	235.4
S_p (MeV)	4.407	5.644	5.644	5.644
E_{QF} (MeV)	177.3	177.7	151.8	206.9
$S_p+E_{xn}+B_{\text{Coul}}$ (MeV)	23.49	23.11	18.6	28.5
$E_{xn}+B_{\text{Coul}}$ (MeV)	19.08	17.47	13.0	22.9
W (MeV)	22.0	22.0	22.0	21.6
E_0 (MeV)	193.829(fixed)	191.656(fixed)	166.0	
T (MeV)	100	100	70	900
$d\sigma/d\Omega(0°)$ (mb/sr)	~233	~273	~10	~2.5
$d\sigma/d\Omega(2°)$ (mb/sr)	~166	~223		
ratio	1.4	1.2		
Breakup/pickup[a]				
$d\sigma/d\Omega(0°)$ (mb/sr)		~12.5		
$d\sigma/d\Omega(2°)$ (mb/sr)		~3.8		
ratio		3.4		

[a] $\frac{d\sigma}{d\Omega} = \int_{150}^{200} \frac{d^2\sigma}{d\Omega dE} dE$.

comparison are the values obtained in the pion charge-exchange experiments (π^+,π^0) on Sn targets [30,31].

Initially all parameters describing the nonresonant continuum background were used as adjustable parameters except for E_0. Only modest variations of the parameters were observed for the two targets and for different boundary conditions (keeping some parameters fixed), thus establishing favored parameters. Also, the shape of the quasifree charge-exchange spectrum is rather insensitive to the parameters. Particularly the dependence on the "temperature" T is weak. Subsequently, only E_{QF} was used as an adjustable parameter, and W, T, and E_0 were fixed at the earlier values. The agreement with the parameters used in pion charge exchange is good except for the cutoff energy E_0 which has been fixed in this work at the three-body breakup energy.

As expected, the cross sections for (^{3}He,t) quasifree charge exchange vary only very little over the angular range from 0° to 2°. The free charge-exchange reaction ^{3}He$(n,p)^3$H has been measured very recently [32] at essentially the same c.m. bombarding energy as in the present experiment. The measured differential cross section at $\theta = 0°$ was found to be ~20 mb/sr. In the present experiment the corresponding differential cross sections for the quasifree charge exchange at $\theta = 0°$ are ~233 mb/sr and ~273 mb/sr for ^{117}Sn and ^{120}Sn, respectively (see Table III). These values divided by the cross sections for the free reaction lead to effective numbers of participating neutrons of ~11.7 and ~13.7, respectively. Assuming that all valence neutrons (with $N \geq 50$) participate in the quasifree process at this bombarding energy, the effective occupation probabilities become ~0.68 for both nuclei. Although a proper comparison can only be made after taking distortion effects into full consideration, it is still worth noting that this result is remarkably close to the occupation probabilities observed in electron-induced proton knockout $(e,e'p)$ from valence shells across the mass table [33] of ~70%.

At increased effective excitation energies of $E_x \gtrsim 30$ MeV, the breakup/pickup reaction provides another source of continuous nonresonant background. Here, the incoming ^{3}He projectile breaks up in the Coulomb field of the target nucleus, $^3\text{He} \rightarrow d+p$. This is followed by a neutron pickup reaction (d,t). Again, the residual nucleus is left in its ground state or an excited single-neutron hole state. This two-step mechanism has characteristics which were studied earlier at $E(^3\text{He}) = 130$ MeV [34,35], leading to the centroid energy $E_{\text{centroid}} \approx \frac{2}{3} E(^3\text{He})$, full width at half maximum (FWHM) $\approx \frac{1}{3} E(^3\text{He})$, and $d\sigma/d\Omega \propto A^{\frac{1}{3}}$. A theoretical description of the process was given by Aarts *et al.* [36] in the plane-wave impulse approximation (PWIA),

$$\frac{d^3\sigma}{dE d\Omega_p d\Omega_t} = |T_{tA}|^2 |\Phi(\mathbf{p}_p - \tfrac{1}{3}\mathbf{p}_{^3\text{He}})|^2 \times (\text{phase space}). \tag{9}$$

Here, p refers to the proton as spectator, T_{tA} is the T-matrix element of the triton-target interaction, $\Phi(p)$ represents the Fourier transform of the relative momentum distribution (Fermi motion) of the p and d inside ^{3}He, and the expression is multiplied by the three-body phase-space factor. If the proton is not detected, the expression has to be integrated over the proton momentum. Figure 8 shows the calculated continuous triton

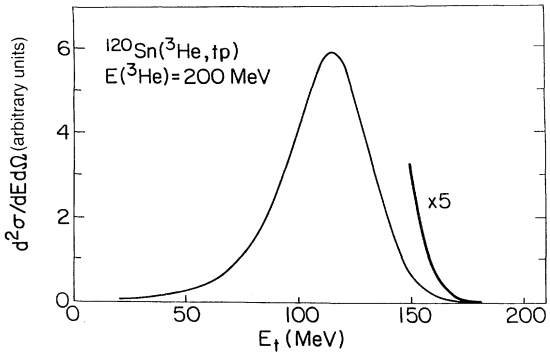

FIG. 8. Theoretical shape of the background continuum from the (^{3}He,dp)(d,t) two-step breakup/pickup reaction mechanism.

spectra for the ^{120}Sn target at the present bombarding energy. The shape of the experimentally observed spectra for ^{120}Sn(^{3}He,t), Fig. 3, with its apparent threshold near $E_x \approx 30$ MeV, is in excellent agreement with the predicted shape. No parameter adjustments were introduced for the shape. However, the magnitude of the yield was taken as a free parameter. The cross sections for $\theta = 0°$ and $\theta = 2°$ integrated for $E_t \geq 150$ MeV and their ratios are included in Table III. The rather strong dependence on angle agrees well with the dependence observed at lower bombarding energies [34,35].

The calculated contributions from quasifree charge exchange and from breakup/pickup with the parameters adjusted as described above are included in Figs. 2 and 3 at both angles and also for the difference spectra $\theta = 0°$–$2°$.

B. Resonance strength and comparison to theoretical calculations

Figures 2 and 3 include several curves which represent the overlapping giant resonance structures obtained from the fitting procedure. The IAS was included in the simultaneous fit of all resonance parameters, but the region of low excitation energies with the discrete states, also shown in Fig. 4, was excluded. Information about these discrete states was extracted directly from the spectra. Gaussian line shapes were assumed in the iterative fitting procedure for the resonances. Initially, a problem developed with the description of the main Gamow-Teller resonance near $E_x \approx 11$ MeV in both ^{117}Sb and ^{120}Sb [19]. It appeared difficult to describe this resonance with a single peak at both angles, $\theta = 0°$ and $2°$. Guided by the theoretical predictions of configuration splitting [5], it was decided to introduce two separate peaks. However, a description using only a single peak for this resonance became possible later by modifying the fitting procedure and by removing correlations between resonance parameters. In order to establish a possible connection with the theoretical predictions, the fits using two separate peaks are also reported below.

Three (in ^{117}Sn) and two (in ^{120}Sn) additional resonances with an $L = 0$ character below the respective IAS's are clearly discernible in the experimental spectra. The amplitudes obtained by independently fitting the difference spectra are in agreement with those obtained from the $0°$ and $2°$ fits. As already mentioned, additional low-lying discrete states which also display $L = 0$ transfer character are seen.

Contributions from the electric giant dipole and/or the spin-flip giant $\Delta L = 1$ resonances, i.e., $L = 1$ with $\Delta S = 0$ and 1, at $E_x \approx 21$ MeV are particularly apparent in the $2°$ spectra. A weak minimum of the cross sections at $0°$ leads to negative amplitudes in the difference spectra ($\theta = 0°$–$2°$). Fitting this structure with a single peak was moderately successful, but certain systematic residuals remained. These made it desirable to introduce two resonances each for ^{117}Sn and ^{120}Sn. Superior agreement with the data could indeed be achieved. It was found later (see below) that the resonance at the higher excitation energies corresponds closely to the expected $T_<$ component of the electric giant dipole resonance, whereas the one at the lower excitation energies may represent the spin-flip $\Delta L = 1$ ($J^\pi = 2^-$) resonance. An additional resonance observed in ^{120}Sb at $E_x \approx 30$ MeV is of unknown origin.

Excitation energies, widths, and $0°$ cross sections, as well as $0°/2°$ cross section ratios were extracted from the analysis and are listed in Tables I and II. While the $0°$ cross sections for the Gamow-Teller resonances are quite reliable and reproducible, the $2°$ cross sections are less reliable, particularly for the GT components near $E_x \approx 12$ MeV, because of the nearby $L = 1$ resonances. The tables also include information for the discrete low-lying states and for the IAS's.

In addition to the IAS's, several low-lying discrete states and several resonances up to $E_x \approx 12$ MeV have $L = 0$ characteristics as deduced from the $0°/2°$ cross section ratios which exceed unity. These states and resonances presumably represent fragments of the collective Gamow-Teller resonance with its main component at $E_x \approx 12$ MeV, i.e., slightly above the IAS's. The rather large cross sections for the resonances in the range $E_x = 3$–7 MeV will be discussed below.

The two resonances observed at $E_x \approx 15$ MeV and 21 MeV do not display $L = 0$ characteristics, and they presumably represent the electric giant dipole and the spin-flip $L = 1$ resonances.

The preceding results show that at $E(^3\text{He}) = 200$ MeV $L = 0$ transitions are clearly observed. Transitions with both non-spin-flip (IAS) and spin-flip (GT) resonances take place. This is expected from the known energy dependence of the effective (and the free) nucleon-nucleon interaction which mediates the (p,n) charge exchange reaction. Numerous (p,n) experiments (e.g., Refs. [17,37–39]), particularly on carbon targets, have established the ratio of spin-flip to non-spin-flip charge exchange. This ratio has a broad maximum at $E(p) \approx 300$ MeV. At $E(^3\text{He}) = 200$ MeV (or 65 MeV/nucleon), both strengths are expected to be about equal if one uses the established correspondence between (p,n) and (^{3}He,t) reactions at the same energy per nucleon.

The various fragments of the Gamow-Teller resonance observed in the present experiment will be given special attention. The upper parts of Figs. 6 and 7 display the observed resonances and the calculated decomposition into components. The spectra were obtained by subtracting the calculated continuous nonresonant background and higher-lying resonances from both the measured and the fitted spectra. The lower parts of Figs. 6 and 7 display the theoretical Gamow-Teller strength functions from Sec. IV of the present work.

The comparison between the observed and theoretical excitation energies for the low-lying Gamow-Teller components shows satisfactory agreement for the excitation energies. Even the predicted presence of several pygmy resonances in ^{117}Sb and ^{120}Sb is confirmed by the data. The centroid energies for the main Gamow-Teller components are also in agreement. However, the theoretically predicted configuration splitting [5] could not be confirmed by the data. The predicted splitting may not exist or it is not observable because the total widths of the main Gamow-Teller components in ^{117}Sb and ^{120}Sb exceed the predicted configuration splitting.

Since the theoretical calculations predict configuration splitting [5], it was decided to perform an independent analysis of the data by introducing two separate peaks near the location of the main Gamow-Teller resonance. The results of this analysis are not included in Figs. 2 and 3. Figures 6 and 7, however, show as dotted lines the results from this analysis. Indeed, two components can be generated with slighly reduced widths. The respective parameters are included in Tables I and II in parentheses. The comparison between the corrected experimental spectra of Figs. 6 and 7 (see also Tables I and II) and the theoretical predictions shows basic agreement for the two centroid energies. However, this agreement establishes only compatibility with theoretical predictions and cannot constitute a definite proof of configuration splitting.

Data obtained more recently for essentially all stable Sn isotopes display significant fragmentation of $L = 0$ strength into separate particle-hole components, often referred to in the literature as direct, core-polarization, and back-spin-flip Gamow-Teller components. The preliminary analysis does not show configuration splitting for any of the targets. The N dependence of the centroid excitation energies of the main Gamow-Teller resonance relative to the IAS's may display a transition from the energetically lower to the energetically higher component near $A = 118$ as predicted [5].

The question arises whether the measured cross sections can be used to deduce experimental Gamow-Teller strengths for comparison with the theoretical strength functions. For (p, n) reactions at bombarding energies exceeding 100 MeV it has been demonstrated [15] that in the plane-wave or distorted-wave impulse approximations the 0° cross sections are proportional to the reduced transition strengths B(GT), and absolute values can be obtained relative to the cross section for the IAS's. Using the measured 0° cross sections and the approximations for the energy dependence of kinematic and distortion effects (e.g., Ref. [37]), one obtains for a bombarding energy of 65 MeV/nucleon the expression $d\sigma/d\Omega(0°;\mathrm{GT})/\ d\sigma/d\Omega(0°;\mathrm{IAS}) \approx 1.47B(\mathrm{GT})/B(\mathrm{IAS})$ with $B(\mathrm{IAS}) = N - Z$. It is assumed here that the noncentral parts of the interaction can be neglected. From the measured cross sections listed in Tables I and II and from Figs. 6 and 7 it becomes immediately clear that this approximation significantly overestimates the values of B(GT) for the low-lying fragments. For example, B(GT) ≈ 0.25 is known for the 1^+ ground state of ^{120}Sb from beta decay measurements. The above equation overestimates this value by a factor of about 7. Also, the summed GT strength would exceed 100% of the sum rule.

The origin of the above behavior lies in the fact that only transitions to the direct Gamow-Teller resonance which are based on collective $j_< j_>^{-1}$ excitations are expected to be dominated by the central interaction $V_{\sigma\tau}$ with $L = 0$ transfer. The lower-lying pygmy resonances contain $j_< j_<^{-1}$, $j_> j_>^{-1}$, and $j_> j_<^{-1}$ excitations, and the wave functions are not necessarily dominated by $L = 0$ spin-flip components. As a consequence, strong contributions from $L = 2$ spin flip are likely to interfere with the $L = 0$ spin-flip contributions. The origin of this effect lies in the existence of the noncentral tensor interaction $V_{T\tau}$.

Detailed ^{12,13,14}C(^{3}He,t)^{12,13,14}N charge-exchange measurements to ground and low-lying states performed very recently suggest a ratio $V_{T\tau}/V_{\sigma\tau}$ on the order of 0.5 at (E^3He) = 200 MeV. A quantitative extraction of reduced transition probabilities B(GT) from the present data has to await improved information from the carbon data about $V_{\sigma\tau}$ and $V_{T\tau}$ as well as structure calculations for both $L = 0$ and $L = 2$ transition densities in the Sn isotopes.

It should be noted, though, that while (^{3}He,t) experiments at $E(^3\mathrm{He})$=200 MeV (limited by the bending power of the magnetic spectrometer) make the extraction of Gamow-Teller strength more difficult, it is the interference effects with $L = 2$ contributions that allow the observation of weak low-lying GT strength residing in the pygmy resonances and discrete states. Very little information about pygmy resonances has come from (p, n) work.

The two resonances observed in the range $E_x = 15$–21 MeV on both targets are not enhanced near $\theta = 0°$. They are believed to represent the $T_<$ components of the non-spin-flip and spin-flip $L = 1$ resonances. In fact, the excitation energies of $E_x = 22.0$ MeV (^{117}Sb) and $E_x = 20.8$ MeV (^{120}Sn) agree very well with the energies predicted from the T_0 components observed in (γ, n) reactions on ^{117}Sn and ^{120}Sn, respectively [40], corrected for the Coulomb displacement and the isospin splitting [13]. The energetically lower $L = 1$ resonances are likely the 2^- components of the spin-flip $L = 1$ resonances.

A resonance in ^{120}Sb at $E_x \approx 30$ MeV is of unknown origin. Its identification with the isovector giant monopole resonance is uncertain and would, in any case, have to be confirmed by coincidence measurements with decay particles. It is interesting to note, though, that the excitation energy is in reasonable agreement with theoretical predictions [41] and results from pion charge exchange [30,31], and we find that the observed cross section agrees with theoretical predictions.

VI. SUMMARY

Triton spectra from the (^{3}He,t) reactions on targets of ^{117}Sn and ^{120}Sn were measured at $E(^3\text{He})$=200 MeV near $\theta = 0°$. Difference spectra for $\theta = 0°$–$2°$ are shown to be a powerful tool for identifying $L = 0$ strength. Interference between the transition strengths from spin-flip charge exchange and the noncentral tensor charge exchange leads to enhanced cross sections for the low-lying particle-hole components including certain discrete states. These interference effects make it therefore possible to observe the low-lying components which are often called "pygmy resonances." These low-lying Gamow-Teller contributions are usually difficult to observe in (p, n) charge exchange.

The observed and theoretically predicted fragmentation of the Gamow-Teller strength are in satisfactory agreement. However, theoretically predicted configuration splitting [5] could not be confirmed, because the observed widths are larger than the predicted splitting, even though the data can be made compatible with the predictions.

The extraction of GT strength from the measured cross sections is more difficult than for (p, n) charge exchange at energies > 100 MeV due to the contributions from the isovector tensor interaction.

ACKNOWLEDGMENTS

The authors acknowledge helpful discussions with M. Fujiwara and K. T. Hecht and the important support by the technical staff of the IUCF, and in particular by W. R. Lozowski. This research was supported in part by the National Science Foundation Grants Nos. PHY-8911831 and PHY-9208468 (UM, Ann Arbor), and PHY-9015057 (IUCF). This work was also part of the research program of the "Stichting voor Fundamenteel Onderzoek der Materie" (FOM) with financial support from the "Nederlandse Organisatie voor Wetenschappelijk Onderzoek" (NWO). The travel Grants Nos. 85-0123 and 90-0219 provided by the Scientific Affairs Division, North Atlantic Treaty Organization, are gratefully acknowledged.

[1] K. Ikeda, S. Fujii, and J. I. Fujita, Phys. Lett. **3B**, 271 (1963); J. I. Fujita and K. I. Ikeda, Nucl. Phys. **67**, 145 (1965).
[2] Yu. V. Gaponov and Yu. S. Lyutostanskii, Yad. Fiz. **19**, 62 (1974) [Sov. J. Nucl. Phys. **19**, 33 (1974)].
[3] Yu. V. Gaponov and Yu. S. Lyutostanskii, Fiz. Elem. Chastits At. Yadra **12**, 1324 (1981) [Sov. J. Part. Nucl. **12**, 528 (1981)].
[4] E. P. Wigner, Phys. Rev. **51**, 106 (1937); **56**, 519 (1939).
[5] V. G. Guba, M. A. Nikolaev, and M. G. Urin, Phys. Lett. B **218**, 283 (1989).
[6] C. Gaarde, K. Kemp, Y. V. Naumov, and P. R. Amundson, Nucl. Phys. **A143**, 497 (1970).
[7] C. Gaarde, K. Kemp, C. Petresch, and F. Folkmann, Nucl. Phys. **A184**, 241 (1972).
[8] C. Gaarde and T. Kammuri, Nucl. Phys. **A215**, 314 (1973).
[9] W. R. Wharton and P. D. Debevec, Phys. Lett. **51B**, 447 (1974); Phys. Rev. C **11**, 1963 (1975).
[10] A. Galonsky, R. R. Doering, D. M. Patterson, and H. W. Bertini, Phys. Rev. C **14**, 748 (1976).
[11] R. R. Doering, A. Galonsky, D. M. Patterson, and G. F. Bertsch, Phys. Rev. Lett. **35**, 1691 (1975).
[12] M. B. Blann, R. R. Doering, A. Galonsky, D. M. Patterson, and F. E. Serr, Nucl. Phys. **A257**, 15 (1976).
[13] W. A. Sterrenburg, S. M. Austin, U. E. P. Berg, and R. DeVito, Phys. Lett. **91B**, 337 (1980).
[14] D. E. Bainum, J. Rapaport, C. D. Goodman, D. J. Horen, C. C. Foster, M. B. Greenfield, and C. A. Goulding, Phys. Rev. Lett. **44**, 1751 (1980).
[15] C. D. Goodman, C. A. Goulding, M. B. Greenfield, J. Rapaport, D. E. Bainum, C. C. Foster, W. G. Love, and F. Petrovitch, Phys. Rev. Lett. **44**, 1755 (1980).
[16] D. J. Horen, C. D. Goodman, C. C. Foster, C. A. Goulding, M. B. Greenfield, J. Rapaport, D. E. Bainum, E. Sugarbaker, T. G. Masterson, F. Petrovitch, and W. G. Love, Phys. Lett. **95B**, 27 (1980).
[17] T. N. Taddeucci, C. A. Goulding, T. A. Carey, R. C. Byrd, C. D. Goodman, C. Gaarde, J. Larsen, D. Horen, J. Rapaport, and E. Sugarbaker, Nucl. Phys. **A469**, 125 (1987).
[18] J. Jänecke, F. D. Becchetti, A. M. van den Berg, G. P. A. Berg, G. Brower, M. B. Greenfield, M. N. Harakeh, M. A. Hofstee, A. Nadasen, D. A. Roberts, R. Sawafta, J. M. Schippers, E. J. Stephenson, D. P. Stewart, and S. Y. van der Werf, Nucl. Phys. **A526**, 1 (1991).
[19] J. Jänecke, in International Conference on Nuclear Structure and Nuclear Reactions at Low and Intermediate Energies, Dubna, Russia, 1992 (unpublished).
[20] H. J. Hofmann, S. Brandenburg, P. Grasdijk, M. N. Harakeh, W. A. Sterrenburg, and S. Y. van der Werf, Nucl. Phys. **A433**, 181 (1985), and references therein.
[21] G. P. A. Berg, L. C. Bland, B. M. Cox, D. DuPlantis, D. W. Miller, K. Murphy, P. Schwandt, K. A. Solberg, E. J. Stephenson, B. Flanders, and H. Seifert, IUCF Scientific and Technical Report, 1986 (unpublished), p. 152.
[22] G. P. A. Berg, L. C. Bland, D. DuPlantis, C. C. Foster, D. W. Miller, P. Schwandt, R. Sawafta, K. A. Solberg, and E. J. Stephenson, IUCF Scientific and Technical Report, 1987–1988 (unpublished), p. 233.
[23] IUCF internal report: XSYS data acquisition software (May 1988, revised April 1990). The original version was developed at Triangle Universities Nuclear Laboratory (TUNL).
[24] V. G. Guba, M. A. Nikolaev, and M. G. Urin, Yad. Fiz. **51**, 973 (1990) [Sov. J. Nucl. Phys. **51**, 662 (1990)].
[25] A. B. Migdal, *Theory of Finite Fermi Systems and Applications to Atomic Nuclei* (Wiley, New York, 1967).
[26] M. H. Urin, Fiz. Elem. Chastits At. Yadra **15**, 109 (1984) [Sov. J. Part. Nucl. **15**, 245 (1984)].

[27] P. Carlos, R. Bergère, H. Beil, A. Leprêtre, and A. Veyssière, Nucl. Phys. **A219**, 61 (1974).
[28] V. G. Soloviev, *The Theory of Atomic Nuclei: Nuclear Models* (Energo Atomizdat, Moscow, 1981).
[29] H. Orihara, G. C. Kiang, S. Nishihara, T. Murakami, T. Nakagawa, K. Furukawa, K. Maeda, K. Miura, S. Adachi, and H. Ohnuma, Phys. Lett. **118B**, 283 (1982).
[30] A. Erell, J. Alster, J. Lichtenstadt, M. A. Monester, J. D. Bowman, M. D. Cooper, F. Irom, H. S. Matis, E. Piasetzki, and U. Sennhauser, Phys. Rev. C **34**, 1822 (1986); A. Erell, Ph.D. thesis, Tel-Aviv University, 1984 (unpublished).
[31] F. Irom, J. D. Bowman, G. O. Bolme, E. Piastzky, U. Sennhauser, J. Alster, J. Lichtenstadt, M. Moinester, J. N. Knudson, S. H. Rokni, and E. R. Siciliano, Phys. Rev. C **34**, 2231 (1986).
[32] A. Celler *et al.*, Phys. Rev. C **47**, 1563 (1993).
[33] L. Lapikàs, Nucl. Phys. **A553**, 297c (1993).
[34] O. Boushid, H. Machner, C. Alderliesten, U. Bechstedt, A. Djaloeis, B. Jahn, and C. Mayer-Böricke, Phys. Rev. Lett. **45**, 908 (1980).
[35] S. Gopal, A. Djalois, J. Bojowald, O. Boushid, W. Oelert, N. G. Puttaswamy, P. Turek, and C. Mayer-Böricke, Phys. Rev. C **23**, 2459 (1981).
[36] E. H. L. Aarts, R. K. Bhowmik, R. J. deMeijer, and S. Y. van der Werf, Phys. Lett. **102B**, 307 (1981).
[37] N. S. P. King, P. W. Lisowski, G. L. Morgan, P. N. Craigh, R. G. Jeppensen, D. A. Lind, J. R. Shepard, J. L. Ullmann, C. D. Zafiratos, C. D. Goodman, and C. A. Goulding, Phys. Lett. B **175**, 279 (1986).
[38] W. P. Alford, R. L. Helmer, R. Abegg, A. Celler, O. Häusser, K. Hicks, K. P. Jackson, C. A. Miller, S. Yen, R. E. Azuma, D. Frekers, R. S. Henderson, H. Baer, and C. D. Zafiratos, Phys. Lett. B **179**, 20 (1986).
[39] B. S. Flanders, R. Madey, B. D. Anderson, A. R. Baldwin, J. W. Watson, C. C. Foster, H. V. Klapdor, and K. Grotz, Phys. Rev. C **40**, 1985 (1989).
[40] B. L. Berman and S. C. Fultz, Rev. Mod. Phys. **47**, 713 (1975).
[41] N. Auerbach and A. Klein, Nucl. Phys. **A395**, 77 (1983).